Available online at www.sciencedirect.com
SCIENCE DIRECT®
Journal of Computational Physics 193 (2004) 697–707
JOURNAL OF COMPUTATIONAL PHYSICS
www.elsevier.com/locate/jcp

Applications of upwind and downwind schemes for calculating electrical conditions in a wire–plate electrostatic precipitator

Hong Lei *, Lian-Ze Wang, Zi-Niu Wu

Department of Engineering Mechanics, Tsinghua University, Beijing 100084, PR China

Received 29 July 2002; received in revised form 18 July 2003; accepted 12 August 2003

Abstract

The traditional finite difference method has been widely used to calculate two-dimensional electrical conditions in the wire–plate electrostatic precipitation and the calculation domain has to be confined in the first quadrant of single discharge electrode on the base of the symmetry assumption. In order to remove the symmetry assumption, an unconditional convergent numerical method, in which the upwind (or downwind) scheme was used for the positive (or negative) corona, is presented to calculate the three-dimensional distributions of the electric potential and the space charge in a wire–plate electrostatic precipitator. And the predicted electric potentials agree well with existing experimental data.

Keywords: Upwind scheme; Downwind scheme; Control-volume method; Electrostatic field; Space charge; Electrostatic precipitator

1. Introduction

The electrostatic precipitator (ESP) is a commonly used device for removing particulates from gas-particulates mixtures exhausted by various industrial processes. The most commonly used electrostatic precipitators are the wire–plate form as shown in Fig. 1. A series of equally spaced vertical corona wires are placed between two vertical parallel plates. The flat plates are grounded and the corona wires are at a high voltage. The corona discharge at these wires causes ions to traverse the interelectrode space to charge dust particles. The charged particles move toward the grounded plates under the influence of the electric field and are deposited on the plates. In the process of particle collection in an electrostatic precipitator, the particle motion is affected by both the electrostatic field and the gas flow.

* Corresponding author. Tel.: +86-10-6279-4155; fax: +86-10-6278-1824.
E-mail addresses: cn_leihong@yahoo.com (H. Lei), wanglz@tsinghua.edu.cn (L.-Z. Wang), ziniuwu@tsinghua.edu.cn (Z.-N. Wu).

0021-9991/$ - see front matter
doi:10.1016/j.jcp.2003.08.016

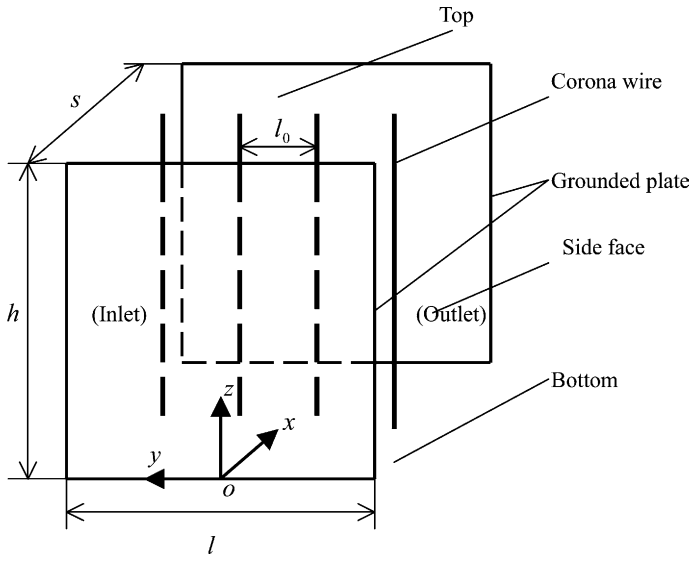

Fig. 1. Schematic of wire–plate electrostatic precipitator.

The electric-field distribution in the ESP is of prime importance for increasing the performance and optimizing the operating conditions of industrial ESP. The electric conditions inside the ESP are determined by the strongly coupled applied electric field and corona-generated space charge (in the absence of particle), and can be described by the steady-state Maxwell equations and a constitutive law relating current and voltage. Assuming that the magnetic field caused by the corona current is negligibly small, the equations defining the electrostatic field in general are

$$\nabla \cdot (\varepsilon_0 \vec{E}) = \rho, \tag{1}$$

$$\nabla \cdot \vec{j} = 0, \tag{2}$$

where

$$\vec{E} = -\nabla V \tag{3}$$

and

$$\vec{j} = \rho \beta \vec{E}, \tag{4}$$

where ε_0 is the permittivity of free space, $\vec{E}$ is the electric-field strength, ρ is the space-charge density, $\vec{j}$ is the current density, V is the electric potential, and β is the ion mobility.

Eq. (3) can be used with Eq. (1) to obtain the Poisson equation for the electric potential:

$$\varepsilon_0 \nabla^2 V = -\rho. \tag{5}$$

Substituting Eqs. (1), (3) and (4) into Eq. (2), the special form of the current continuity equation involving V and ρ is generated:

$$\nabla \cdot \vec{j} = \nabla \cdot (\rho \beta \vec{E}) = \rho \beta \nabla \cdot \vec{E} + \beta \vec{E} \cdot \nabla \rho + \rho \vec{E} \cdot \nabla \beta = \rho \beta (\rho / \varepsilon_0) + \beta (-\nabla V) \cdot \nabla \rho + \rho (-\nabla V) \cdot \nabla \beta = 0. \tag{6}$$

In this work, β is a const., that is $\nabla\beta = 0$. Therefore, Eq. (6) can be expressed as follows:

$$\varepsilon_0 \nabla V \cdot \nabla \rho = \rho^2. \tag{7}$$

The traditional finite difference method (FDM), described in the following section, has been widely used to solve the Poisson equation (5) and the current continuity equation (7) [1,2]. However, all these authors used two-dimensional, symmetric domains [1–8], but did not investigate if these assumptions were reasonable. Nor did they consider why the calculation domain had to be the first quadrant of single discharge electrode or why the forward difference scheme could not be applied to get the space-charge density gradient in the traditional FDM.

Because the electrical equations are analogous to the equations used to describe fluid flow, the downwind scheme, which is customarily used to treat the fluid dynamics problems [9], is introduced in this paper to solve the current continuity equation in the case of positive corona, and the relevant upwind scheme is used in the case of negative corona. As a consequence, the symmetry assumptions can be removed, and the governing equation can be solved to describe the three-dimensional unsymmetrical electrical conditions in the whole ESP in an unconditionally convergent way. In this method, the semi-empirical expression proposed by Peek [10] is introduced to describe the space-charge density near the corona wire, and the first-order upwind (or downwind) scheme is applied to the current continuity equation, and the second-order central differential scheme is applied to the Poisson's equation for electric potential.

In the rest of this paper, we analyze the reason why the traditional FDM only converges in the first quadrant of single discharge electrode and gives the numerical method suitable for obtaining a convergence solution in the other quadrants (Section 2). Based on an analogy between the electric equation and the fluid dynamics equation, we propose a numerical method to solve the Poisson's equation for electric potential and the current continuity equation and prove the convergence of this method. Finally, we will perform numerical computations and compare the predicted result with the experimental data (Section 3).

2. Traditional finite difference method and its limitation

In the traditional FDM, the central difference scheme is used for the electric potential and the backward difference scheme is used for the gradient of the space-charge density [1–8] as follows:

$$E_x = -\frac{\partial V}{\partial x} = \frac{V_W - V_E}{(\delta x)_e + (\delta x)_w}, \quad E_y = -\frac{\partial V}{\partial y} = \frac{V_S - V_N}{(\delta y)_n + (\delta y)_s},$$

$$\left.\frac{\partial \rho}{\partial x}\right|_{-1/2} = \frac{\rho_P - \rho_W}{(\delta x)_w}, \quad \left.\frac{\partial \rho}{\partial y}\right|_{-1/2} = \frac{\rho_P - \rho_S}{(\delta y)_s},$$

where δx and δy are mesh sizes in x and y, respectively. The geometry is shown in Fig. 2. For the simplest condition, the computational domain can be divided into four zones, as shown in Fig. 3.

Now we explain the reason why the traditional FDM complies with the physical fact in the zone I. If the backward difference scheme is used for the gradient of the space-charge density, the space charge at grid point P is determined by the information at the neighbors W and S, not at the other neighbors E and N. Thus, the grid point in the upstream side should provide the full information for the grid point in the downstream in this scheme. Here, the upstream side and the downstream side are based on the direction of the coordinate system. This requires the space charges to move in the positive direction of the coordinate system. For the positive corona, the direction of the electric-field strength and the positive direction of the coordinate system are the same in domain I, so the traditional FDM complies with the physical rule that the

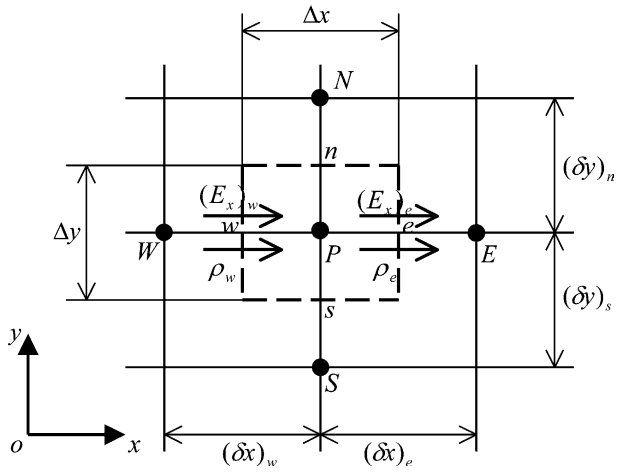

Fig. 2. Control volume for the two-dimensional geometry.

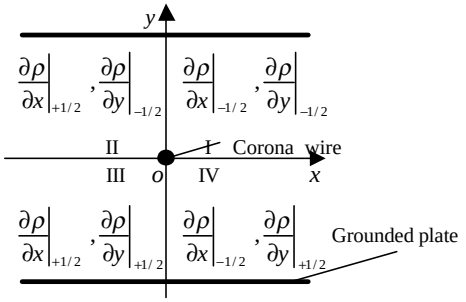

Fig. 3. Convergence domain for traditional finite difference method: +1/2 forward difference scheme; +1/2 downward difference scheme.

positive charges move in the direction of the electric-field strength. Thus, the converged numerical solution can be obtained by the traditional FDM in domain I.

However, in order to comply with the physical rules in zone III, the space charge at grid point P should be determined by that at the neighbors E and N, so it conflicts with the backward difference scheme. Such a conflict also occurs in zones II and IV.

If we want to obtain the converged solution in zone II, III or IV, the corresponding difference scheme for the gradient of the space charge density should be defined as follows:

Zone II. Forward difference scheme for $\partial\rho/\partial x$, and backward difference scheme for $\partial\rho/\partial y$.

Zone III. Forward difference scheme for $\partial\rho/\partial x$, and forward difference scheme for $\partial\rho/\partial y$.

Zone IV. Backward difference scheme for $\partial\rho/\partial x$, and forward difference scheme for $\partial\rho/\partial y$.

For the negative corona, the direction of the electric field is opposite to that of the positive corona, and the negative charges move in the opposite direction of the electric-field strength. Therefore, the direction of the charge motion is the same in the same domain independent of the corona charge. On this condition, the backward difference scheme can still be successfully applied to domain I, and the forward difference scheme can also be successfully applied to domain III. Schemes for the gradient of the space-charge density that ensure relative convergent calculations in all the domains are shown in Fig. 3.

In conclusion, the traditional FDM does not follow the directions of the electric-field strength in all zones so that its applications are limited.

3. Control-volume method and numerical experiment

We make an analogy between the fluid flow problem and the electric-field problem in order to apply the well-established numerical approach for fluid flow to the present problem of electric field. Consider a steady and incompressible flow governed by the continuity equation, the momentum balance equation and the energy equation which can be uniformly written as

$$\rho_{\mathrm{f}}\vec{u}_{\mathrm{f}}\cdot\nabla(\phi)+\nabla\cdot(\Gamma\nabla\phi)=S \tag{8}$$

where ρ_{f} is the fluid density, $\vec{u}_{\mathrm{f}}$ is the fluid velocity, Γ is the diffusion coefficient. The terms and coefficients in this expression depend on the dependent variable, ϕ. The three terms in the general differential equation are the convection term, the diffusion term and the source term, S. In order to compare with Eq. (8), we rewrite Eqs. (5) and (7) as

$$\nabla\cdot(\varepsilon_0\nabla V)=-\rho, \tag{9}$$

$$\varepsilon_0\vec{E}\cdot\nabla\rho=-\rho^2. \tag{10}$$

The Poisson's equation for the electric-potential equation (9) has a diffusion term and a source term, and the current continuity equation (10) has a convection term and a source term. Therefore, we can apply the control-volume method, which is widely applied in the computational fluid dynamics, to the calculation of the distributions of the electric potential and the space charge in the ESP.

3.1. Poisson's equation for electric potential

Using the standard method for the discretization of the diffusion term and the source term, the derivative ∇V in Eq. (9) can be evaluated from a piecewise-linear profile, with the integrated equation over the control volume shown in Fig. 2 being defined by

$$\frac{V_E-V_P}{\Delta x(\delta x)_e}-\frac{V_P-V_W}{\Delta x(\delta x)_w}+\frac{V_N-V_P}{\Delta y(\delta y)_n}-\frac{V_P-V_S}{\Delta y(\delta y)_s}+\frac{V_T-V_P}{\Delta z(\delta z)_t}-\frac{V_P-V_B}{\Delta z(\delta z)_b}=-\rho_P/\varepsilon_0, \tag{11}$$

where ρ_P is the average space volume charge density in the control volume, P. The discretization equation (11) can be cast into the following form:

$$a_PV_P=a_EV_E+a_WV_W+a_NV_N+a_SV_S+a_TV_T+a_BV_B+b, \tag{12}$$

where

$$a_E=\frac{1}{\Delta x(\delta x)_e},\quad a_W=\frac{1}{\Delta x(\delta x)_w},\quad a_N=\frac{1}{\Delta y(\delta y)_n},\quad a_S=\frac{1}{\Delta y(\delta y)_s},\quad a_T=\frac{1}{\Delta z(\delta z)_t},\quad a_B=\frac{1}{\Delta z(\delta z)_b},$$

$$a_P=a_E+a_W+a_N+a_S+a_T+a_B,\quad b=\rho_P/\varepsilon_0.$$

3.2. Current continuity equation

The current continuity equation does not have a diffusion term, so the current continuity equation is parabolic. Namely, the charge motion is unidirectional with the positive charges moving from upstream to downstream and the negative charges moving from downstream to upstream. Here, the upstream side and the downstream side are based on the direction of the electric field. For the positive charge, the

space-charge density at each point is affected by the upstream conditions. Therefore, the upwind scheme can be applied to describe the space-charge distribution for the positive corona. The forward and backward difference schemes for the electric potential, V, were used to calculate the electric-field strength, $\vec{E}$, across the control-volume faces as shown in Fig. 2.

Integration of Eq. (10) over the control volume gives

$$(E_x)_e A_e \rho_e - (E_x)_w A_w \rho_w + (E_y)_n A_n \rho_n - (E_y)_s A_s \rho_s + (E_z)_t A_t \rho_t - (E_z)_b A_b \rho_b = -\rho_P^2 \Delta v/\varepsilon_0, \tag{13}$$

where ρ_i $(i = e, w, n, s, t, b)$ represents the value of ρ at the control-volume face, A_i is the area of the control-volume face, and $\Delta v = \Delta x \Delta y \Delta z$ is the volume of the control volume P.

As a result, the space-charge density at a grid point should be determined by the direction of the electric field and the sign of the space charge. For the positive corona, the direction of the electric-field strength and the positive ion motion are the same. Thus, the upwind scheme should be applied to assure that the space-charge density at the interface is equal to that of the grid point on the upstream side.

Thus,

$$\rho_e = \begin{cases} \rho_P & \text{if } (E_x)_e > 0, \\ \rho_E & \text{if } (E_x)_e < 0. \end{cases}$$

The values of ρ_w, ρ_n, ρ_s, ρ_t and ρ_b are defined similarly. Then, Eq. (13) can be rewritten as

$$a_P \rho_P = a_E \rho_E + a_W \rho_W + a_N \rho_N + a_S \rho_S + a_T \rho_T + a_B \rho_B + b, \tag{14}$$

where

$$a_E = \max[-(E_x)_e A_e, 0], \quad a_W = \max[(E_x)_w A_w, 0], \quad a_N = \max[-(E_y)_n A_n, 0],$$

$$a_S = \max[(E_y)_s A_s, 0], \quad a_T = \max[-(E_z)_t A_t, 0], \quad a_B = \max[(E_z)_b A_b, 0],$$

$$a_P = a_E + a_W + a_N + a_S + a_T + a_B + [(E_x)_e A_e - (E_x)_w A_w + (E_y)_n A_n - (E_y)_s A_s + (E_z)_t A_t - (E_z)_b A_b],$$

$$b = -\rho_P^2 \Delta V/\varepsilon_0.$$

However, for the negative corona, the direction of the electric-field strength is opposite to that of the negative charge motion. Thus, the downwind scheme should be applied to assure that the space-charge density at the interface is equal to that of the grid point on the downstream side.

Thus,

$$\rho_e = \begin{cases} \rho_E & \text{if } (E_x)_e > 0, \\ \rho_P & \text{if } (E_x)_e < 0. \end{cases}$$

The values of ρ_w, ρ_n, ρ_s, ρ_t and ρ_b are defined similarly. Then, Eq. (13) can be rewritten as

$$a_P \rho_P = a_E \rho_E + a_W \rho_W + a_N \rho_N + a_S \rho_S + a_T \rho_T + a_B \rho_B + b, \tag{15}$$

where

$$a_E = \max[(E_x)_e A_e, 0], \quad a_W = \max[-(E_x)_w A_w, 0], \quad a_N = \max[(E_y)_n A_n, 0],$$

$$a_S = \max[-(E_y)_s A_s, 0], \quad a_T = \max[(E_z)_t A_t, 0], \quad a_B = \max[-(E_z)_b A_b, 0],$$

$$a_P = a_E + a_W + a_N + a_S + a_T + a_B - [(E_x)_e A_e - (E_x)_w A_w + (E_y)_n A_n - (E_y)_s A_s + (E_z)_t A_t - (E_z)_b A_b],$$

$$b = \rho_P^2 \Delta V/\varepsilon_0.$$

3.3. Convergence

The algorithm will converge if it satisfies the following three basic rules [9].

(1) When a face is common to two adjacent control volumes, the flux across it must be represented by the same expression in the discretization equations for the two control volumes.
(2) The coefficient a_P at the grid point P and the neighbor coefficients a_{nb} $(nb = E, W, N, S, T, B)$ must always be positive.
(3) The coefficient at the grid point P must be always equal to or greater than the sum of the neighbor coefficients (E, W, N, S, T, B).

Clearly, the discretized Poisson's equation for the electric potential, Eq. (12), satisfies the above three basic rules and the discretized equations for the current continuity equation, Eqs. (14) and (15) satisfy the rules (1) and (2).

Now let us show that Eqs. (14) and (15) also satisfy the rule (3). For this purpose, were write Eq. (9) as $\nabla \cdot \vec{E} = \rho/\varepsilon_0$. Integration over the control volume gives

$$(E_x)_e A_e - (E_x)_w A_w + (E_y)_n A_n - (E_y)_s A_s + (E_z)_t A_t - (E_z)_b A_b = \rho_P \Delta V/\varepsilon_0. \tag{16}$$

For the positive corona, $\rho > 0$, we have

$$(E_x)_e A_e - (E_x)_w A_w + (E_y)_n A_n - (E_y)_s A_s + (E_z)_t A_t - (E_z)_b A_b > 0. \tag{17}$$

For the negative corona, $\rho < 0$, we obtain

$$-[(E_x)_e A_e - (E_x)_w A_w + (E_y)_n A_n - (E_y)_s A_s + (E_z)_t A_t - (E_z)_b A_b] = (-\rho_P)\Delta V/\varepsilon_0 > 0. \tag{18}$$

Hence, a_P is always greater than $a_E + a_W + a_N + a_S + a_T + a_B$, for both positive and negative coronas, so Eqs. (14) and (15) always satisfy the third rule.

3.4. Boundary conditions and convergence criteria

The boundary conditions used in this calculation are summarized in Table 1. According to the semi-empirical formula by Peek [10], the space-charge density near the wire, ρ_W, can be given by:

$$\rho_W = \frac{l_0 j_P}{\pi \beta r f [30\delta + 0.9(\delta/r)^{1/2}]} \times 10^{-5}, \tag{19}$$

where l_0 is the wire–wire spacing, j_P is the average current density at the grounded plate, r is the corona wire radius, f is the roughness factor of the corona wire, δ is $T_0 P/T P_0$, T_0 is 293 K, P_0 is 1.01×10^5 Pa, and P and T are the operating pressure and temperature [2,3]. The calculational domain was discretized using a nonuniform grid of 146 (longitudinal) $\times$ 13 (vertical) $\times$ 52 (traverse) elements with a densely packed grid near the corona wire to represent the strong gradient of the electric field as shown in Fig. 4. The discretized equations for V and ρ were solved using the tri-diagonal matrix algorithm coupled with the Gauss–Siedel routine. In order to avoid divergence in the iterative solution, underrelaxation was employed.

Table 1
Boundary conditions

	Grounded plate	Corona wire	Side face, top, bottom
Electric potential	$V = 0$	$V = -46.2$ kV	$\partial V/\partial n = 0$
Space-charge density	$\partial \rho/\partial n = 0$	$\rho = \rho_W$	$\partial \rho/\partial n = 0$

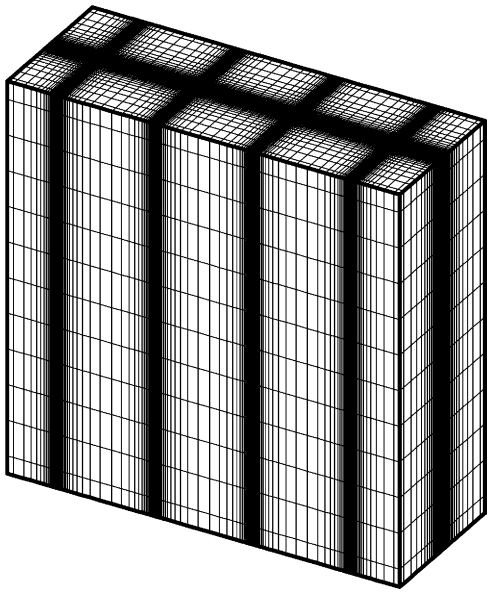

Fig. 4. Computational mesh.

The numerical solution of Eqs. (9) and (10) was performed in the following sequences.

1. Solve Eq. (9) with an initial guess of free space charge.
2. Apply the upwind (or downwind) scheme for the positive (or negative) corona.
3. Assume the space-charge density at the corona wire.
4. Calculate the electric field from Eq. (3).
5. Calculate the current continuity equation (10).
6. Calculate the Poisson equation for the electric potential.
7. Return to step (4) and repeat until convergence.

The convergence criteria are

$$\max\left|\frac{V^{*(K+1)}-V^{*(K)}}{V^{*(K+1)}}\right|<10^{-6}, \tag{20}$$

$$\max\left|\frac{\rho^{*(K+1)}-\rho^{*(K)}}{\rho^{*(K+1)}}\right|<2\times10^{-5}, \tag{21}$$

where K is the iteration number.

The program was compiled by Fortran 77, and run on a PC1.8G/256M. About 500 over all iterations were required to attain the bounds in Eqs. (21) and (22), and 10 iterations were required to solve Poisson equation in each overall iteration.

3.5. Numerical experiments

The computational results were compared with the experimental data of Penny and Matick [11]. Their experimental conditions are summarized in Table 2. The electric mobility of gas ions, β, was assumed to be $1.8\times10^{-4}\ \mathrm{m^2\,V^{-1}\,s^{-1}}$, which is typical for a negative corona [2,3].

Table 2
Experimental conditions

Wire-to-wire spacing	$l_0 = 152.4$ mm	Plate-to-plate space	$s = 228.6$ mm
Wire length	$h = 609.6$ mm	Plate length	$l = 609.6$ mm
Wire radius	$r = 1$ mm		

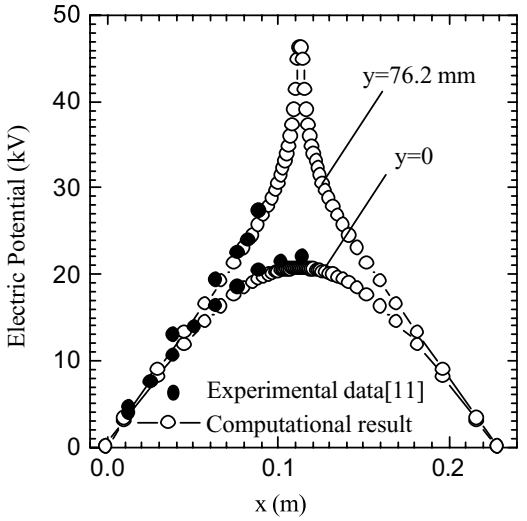

Fig. 5. Comparisons of the predicted electric potential with published experimental data.

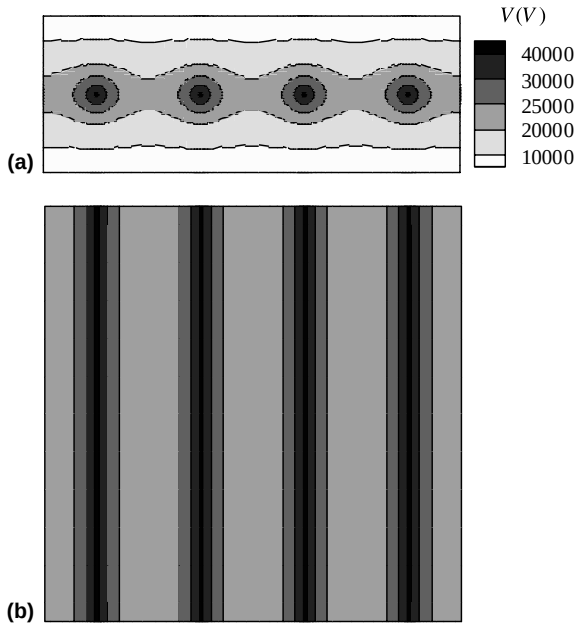

Fig. 6. Spatial distribution of electric potential in the wire–plate ESP: (a) horizontal distribution at the central plane and (b) vertical distribution at the central plane.

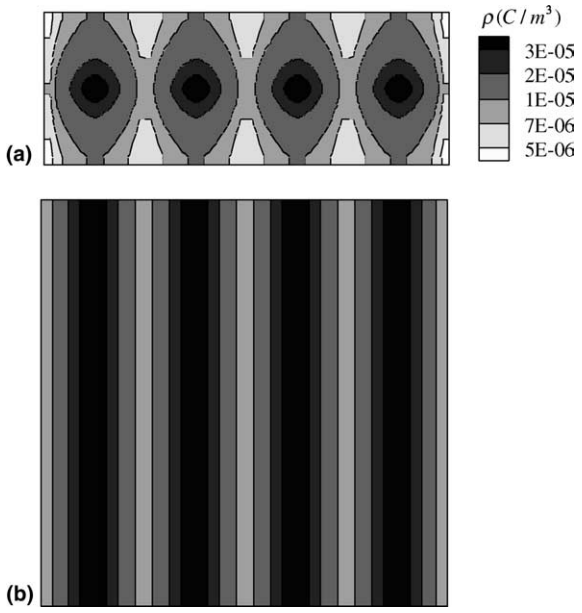

Fig. 7. Spatial distribution of space-charge density in the wire–plate ESP: (a) horizontal distribution at the central plane and (b) vertical distribution at the central plane.

Fig. 5 shows that the predicted voltage distribution agreed well with the experimental data [11]. The maximum relative error was about 12% because the data in [11] could not be measured exactly. The electric potentials shown on the curve, as with all the electric potentials in this paper were negative, but were not designated as such.

Figs. 6 and 7 show the three-dimensional distributions of the electric potential and the space-charge density.The horizontal distributions for the electric potential and the space-charge density have an annular shape, with the corona wires being located at the center of the annulus. The influences of the inlet and outlet were not great, as shown in Fig. 7(a), therefore, periodic boundary conditions were applied as an approximation. Fig. 7(b) shows that all the isometric lines for the electric potential and the space-charge density were parallel to the corona wire. So, along the direction of the corona wire, the distributions of the electric potential and the space charge are the same, therefore, the distributions of the electric potential and the space charge in the wire–plate electrostatic precipitator can be analyzed as two-dimensional.

4. Conclusion

The electrical condition in an electrostatic precipitator is a three-dimensional unsymmetrical problem, but the traditional FDM is based on the two-dimensional symmetrical assumption. Thus, an unconditional convergent numerical method is presented here to solve the three-dimensional unsymmetrical problem. The present method complies with the physical facts that the positive charges move in the direction of the electric-field strength and the negative charges move in the opposite direction of the electric-field strength, so it can be applied without knowing the electric-field direction a priori by using the upwind (or downwind) scheme for the positive (or negative) corona. Comparisons of the predicted electric potential with existing experimental data indicated that the numerical method could be used to design electrostatic precipitators with the wire–plate geometry.

Acknowledgements

This work was supported by the Natural Science Foundation of Beijing (No. 8012010), Tsinghua Basic Science Foundation (No. 200114006), China Postdoctoral Science Foundation (No. 200217) and Chinese National Natural Science Foundations (No. 10025210).

References

[1] G. Leutert, B. Bohlen, Der raumliche verlauf von elektrischer feldstarke und raumladungsdichte im platten-elektrofilter, Staub Reinhalt Luft. 32 (7) (1972) 297–301.
[2] J.R. McDonald, W.B. Smith, H.W. Spencer III, L.E. Sparks, A mathematical model for calculating electrical conditions in wire-duct electrostatic precipitation devices, J. Appl. Phys. 48 (6) (1977) 2231–2243.
[3] C. Lu, H. Huang, A sectional model to predict performance of a plate-wire electrostatic precipitator for collecting polydisperse particles, J. Aerosol Sci. 29 (3) (1998) 295–308.
[4] J.H. Goo, J.W. Lee, Stochastic simulation of particle charging and collection characteristics for a wire–plate electrostatic precipitator of short length, J. Aerosol Sci. 28 (5) (1997) 875–893.
[5] S.J. Park, S.S. Kim, Electrohydrodynamic flow and particle transport mechanism in electrostatic precipitator with cavity walls, Aerosol Sci. Tech. 33 (3) (2000) 205–221.
[6] F.C. Lai, P.J. Mckinney, J.H. Davidson, Oscillatory electrohydrodynamic gas flows, J. Fluid Eng. 117 (9) (1995) 491–495.
[7] A. Soldati, On the effects of electrohydrodynamic flows and turbulence on aerosol transport and collection in wire–plate electrostatic precipitators, J. Aerosol Sci. 31 (3) (2000) 293–305.
[8] T. Yamamoto, H.R. Velkoff, Electrohydrodynamics in an electrostatic precipitator, J. Fluid Mech. 108 (1981) 1–18.
[9] S.V. Patankar, Numerical Heat Transfer and Fluid Flow, Hemisphere, Washington, 1980.
[10] F.W. Peek, Dielectric Phenomena in High-Voltage Engineering, McGraw-Hill, NewYork, 1929.
[11] G.W. Penney, R.E. Matick, Potentials in dc corona fields, Trans. AIEE 79 (5) (1960) 91–99.